JACS
JOURNAL OF THE AMERICAN CHEMICAL SOCIETY
Article
pubs.acs.org/JACS

Multifunctional Envelope-Type Mesoporous Silica Nanoparticles for Tumor-Triggered Targeting Drug Delivery

Jing Zhang, Zhe-Fan Yuan, Ya Wang, Wei-Hai Chen, Guo-Feng Luo, Si-Xue Cheng, Ren-Xi Zhuo, and Xian-Zheng Zhang*

Key Laboratory of Biomedical Polymers of Ministry of Education and Department of Chemistry, Wuhan University, Wuhan 430072, P. R. China

Supporting Information

ABSTRACT: A novel type of cellular-uptake-shielding multifunctional envelope-type mesoporous silica nanoparticle (MEMSN) was designed for tumor-triggered targeting drug delivery to cancerous cells. β-Cyclodextrin (β-CD) was anchored on the surface of mesoporous silica nanoparticles via disulfide linking for glutathione-induced intracellular drug release. Then a peptide sequence containing Arg-Gly-Asp (RGD) motif and matrix metalloproteinase (MMP) substrate peptide Pro-Leu-Gly-Val-Arg (PLGVR) was introduced onto the surface of the nanoparticles via host−guest interaction. To protect the targeting ligand and prevent the nanoparticles from being uptaken by normal cells, the nanoparticles were further decorated with poly(aspartic acid) (PASP) to obtain MEMSN. *In vitro* study demonstrated that MEMSN was shielded against normal cells. After reaching the tumor cells, the targeting property could be switched on by removing the PASP protection layer via hydrolyzation of PLGVR at the MMP-rich tumor cells, which enabled the easy uptake of drug-loaded nanoparticles by tumor cells and subsequent glutathione-induced drug release intracellularly.

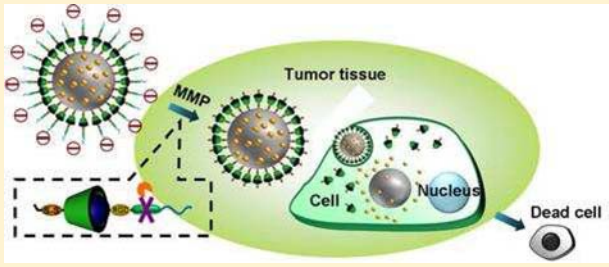

INTRODUCTION

For cancer therapy, drug delivery manner plays an important role in the anticancer efficacy of medicinally active molecules.[1] Since traditional antineoplastic drugs can not discern between diseased and healthy cells, the drug dose within cancerous cells is always limited, and systemic toxicity with undesired side effects is inevitable. In order to improve the therapeutic index of drugs in cancer therapy, enormous research efforts have been made to develop ideal drug carriers for tumor-targeted drug delivery. However, there are several obstacles during the transporting process of drug delivery systems to tumoral cells, such as the aggregation and rapid clearance during the circulation, and unspecific uptake of normal cells. To overcome these barriers, an ideal drug carrier should combine a variety of functions, such as protection to keep the carrier stable and avoid nonspecific cell uptake, tumor-targeting ability to accumulate at tumor sites, ligand-mediated cell adhesion for efficient cellular entry, and effective drug encapsulation to permit the drug release inside tumoral cells only.

Recently, a new concept of "programmed packaging" or "multifunctional envelope-type nanodevice (MEND)" was proposed to overcome various barriers in the process of gene delivery to nucleus of target cells.[2] In MEND, the plasmid DNA is condensed by a polycation and then coated with a lipid bilayer, analogous to envelope-type viruses. Then the functional components, such as specific ligands to enhance cell uptake and fusogenic lipids to fuse with the endosomal membrane, are introduced into the bilayer. Compared with conventional delivery systems, MEND possesses unique advantages because the assembled functional components exert their specific functions at appropriate sites as well as at the right time for the optimum intracellular pharmacokinetics and pharmacodynamics. Inspired from the concept of MEND, we designed and fabricated a multifunctional envelope-type drug carrier, which can overcome the intricate barriers during the drug-transporting process for targeted drug delivery in cancerous cells.

It is well documented that the surface charge of the drug carriers has serious impact on their fate *in vitro* and *in vivo*.[3] Positively charged nanoparticles may cause severe aggregation and rapid clearance from circulation due to the strong interactions with serum components, which restrict their potential applications *in vivo*.[4−6] In contrast, negatively charged carriers are favorable for protein resistance.[7] Moreover, negatively charged nanoparticles exhibit prolonged circulation time during applications.[8,9] In our previous research, we also demonstrated that polyanionic carriers could avoid unspecifically cell uptake.[10] Thus, drug delivery systems with polyanion outer layers have several favorable features, including enhanced stability in physiological conditions and prolonged circulation time in blood.

Although the negatively charged outer layers of the drug delivery systems are favorable to prolong the systemic circulation time and thus to achieve passive targeting at

Received: December 9, 2012
Published: March 6, 2013

   dx.doi.org/10.1021/ja312004m | J. Am. Chem. Soc. 2013, 135, 5068−5073

tumor sites due to the enhanced permeability and retention (EPR) effect, the negatively charge surfaces have an unfavorable effect on the cell uptake at the targeted sites. To address this issue, it is highly desirable to fabricate polyanion-protected drug carriers that can change their surface property and become recognizable by cancerous cells after arriving at the targeted tumor sites. In other words, the carriers should have a "tumor-triggered targeting" property. As far as we know, drug carriers with tumor-triggered targeting properties remain scarcely investigated.

To achieve a tumor-triggered targeting property, a tumor localization signal (TLS) which can trigger the switch of the surface property of drug carriers is critically important. Several TLSs were reported to remove the protection layer and expose the protected targeting ligands in response to the acidic environment of tumor. For example, Wang et al. developed ternary nanoparticles for tumor acidity-targeted siRNA delivery. With a specific response to tumor acidity, the nanoparticles showed enhanced uptake by tumor cells and improved delivery efficiency of siRNA in cancer therapy.[11] In our previous study, we also reported fluorescent drug carriers with the ability to remove the PEG stealth layer at a pH < 6.8 and expose the RGD-targeting motif for improved uptake by tumor cells.[12] However, in practical applications, the pH difference between tumor sites and normal tissues may not be sufficient to trigger the deshielding process. As we know, the abnormal increase of the matrix metalloproteinases (MMPs) is intimately associated with tumor invasiveness, metastasis, and angiogenesis.[13−16] Since MMPs are overexpressed in the extracellular environment of certain kinds of tumors, MMPs can be used as a kind of TLS in cancer therapy. To design tumor-triggered targeting drug carriers which can respond to MMP is of clinical importance.

Moreover, traditional drug carriers always suffer from unexpected drug release during circulation. Ideal drug carriers should be able to encapsulate drugs efficiently before reaching tumor sites. In this regard, mesoporous silica nanoparticles (MSN) as drug carriers have their unique advantages.[17−19] In addition to their stable mesoporous structures, large surface area, tunable pore sizes, and well-defined surfaces,[20] which are favorable for drug loading, MSN can be further coated with a monolayer of gatekeepers. For example, cyclodextrin (CD) gated MSN are able to efficiently entrap different cargos in the pores and allow the release of cargos from the pores until a specific external trigger emerges, such as redox potenial,[21] pH,[22] light,[23] and enzymes.[24]

In this study, we fabricated a novel type of multifunctional envelope-type mesoporous silica nanoparticle (MEMSN) to achieve the tumor-triggered targeting drug delivery in a so-called "programmed packing" manner. As illustrated in Scheme 1, doxorubicin hydrochloride (DOX), an anticancer drug, was loaded in the mesoporous silica core with the surface linked with β-CD through disulfide bonding. The nanoparticle was further decorated with RGD and PLGVR peptides and a polyanion (PASP). The polyanion protection layer can avoid the nonspecific uptake under physiological conditions. After the nanoparticle arrives at tumor sites, the polyanion protection outer layer can be removed via the hydrolyzation of the MMP substrate peptide (PLGVR),[25] leading to the exposing of the targeting RGD motif. Thereafter, the nanoparticle would be uptaken by a tumor cell, and the drug could be released quickly from the nanoparticle since the CD gatekeeper can be removed due to the breakage of disulfide linkers induced by concentrated glutathione (GSH) inside the tumor cell.[20,26,27]

Scheme 1. Structure of MEMSN and Tumor-Triggered Targeting Drug Delivery[a]

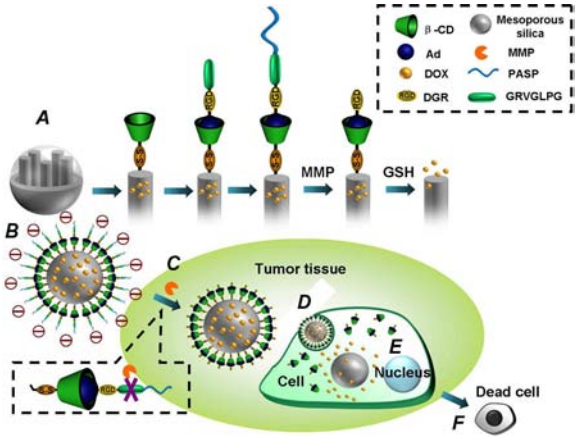

[a](A) Functionalization protocol of the MSN; (B) drugs loaded MEMSN under physiological condition; (C) removal of PASP protection layer in response to MMP at a tumor site; (D) cell uptake through RGD-mediated interaction; (E) glutathione-triggered drug release inside the cell; and (F) apoptosis of tumor cells.

RESULTS AND DISCUSSION

In this study, we synthesized MSN with an average diameter of ~140 nm, as shown in the scanning electron microscopy (SEM) and transmission electron microscopy (TEM) images in Figure 1A,C. The highly ordered lattice array indicated a uniform, well-defined mesostructure of the obtained MSN, which was further characterized by X-ray diffraction (XRD) analysis (Figure 1B). The surface functionalization of MSN was characterized by FT-IR (Figure S1). As shown in Scheme S1, the surface of MSN was first functionalized with 3-mercaptopropyltrimethoxysilane to obtain MSN-SH. The FT-IR spectrum of MSN-SH showed a thiol absorption band at 2560 cm^{-1}. Thereafter, MSN-SS-NH_2 was synthesized, which reacted with propargyl bromide to produce MSN-SS-alkyne. The typical absorption peak of alkyne moiety at 2125 cm^{-1} proved the successful functionalization of alkyne moieties.

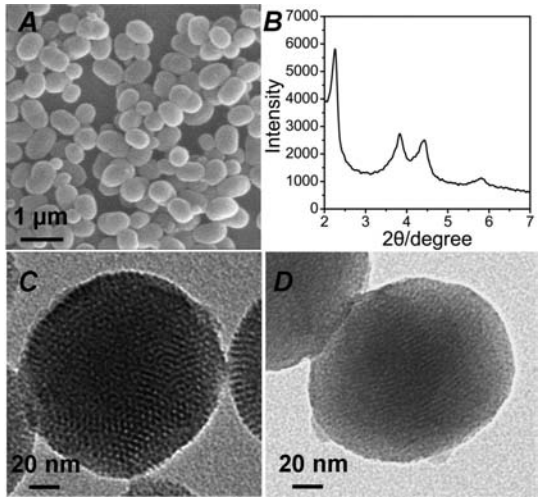

Figure 1. (A) SEM image of MSN; (B) low-angle XRD pattern of MSN; (C) TEM images of MSN; and (D) TEM image of DOX-loaded MSN-SS-CD-peptide-PASP.

dx.doi.org/10.1021/ja312004m | J. Am. Chem. Soc. 2013, 135, 5068−5073

Then the surfactant template hexadecyl trimethyl ammonium bromide (CTAB) was removed from MSN-SS-alkyne by refluxing with a solution containing MeOH and HCl. DOX was loaded into the pores of the nanoparticles by vigorous stirring the mixture of MSN-SS-alkyne nanoparticles and DOX solution for 24 h. Subsequently, the gatekeeper β-CD was immobilized onto DOX loaded or unloaded MSN-SS-alkyne via "click chemistry" between mono-6-azido-β-CD and MSN-SS-alkyne to obtain MSN-SS-CD. As shown in the thermal gravimetric analysis (TGA) curves in Figure 2, the weight loss

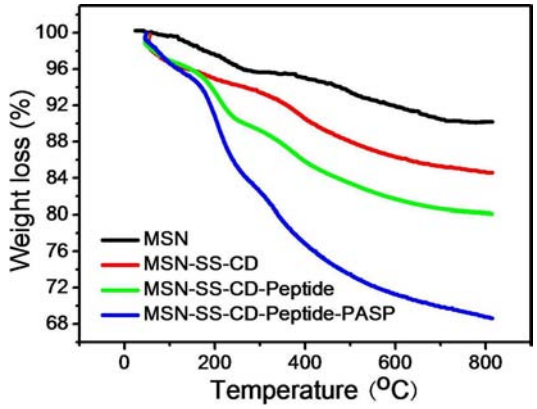

Figure 2. TGA curves of different nanoparticles: MSN, MSN-SS-CD, unloaded MSN-SS-CD-peptide, and unloaded MSN-SS-CD-peptide-PASP.

values of unloaded MSN-SS-CD and MSN were 15.5% and 9.8%, respectively, when the temperature increased to 800 °C. The increased weight loss of unloaded MSN-SS-CD indicated that β-CD was successfully immobilized onto the surface of the nanoparticles.

To achieve tumor-triggered targeting, a tumor-targeting ligand and a tumor environment-triggered cleavable linker were introduced onto MSN-SS-CD. It is well-known that integrin receptors are overexpressed[28−30] in various cancer cells, and the RGD motif could specifically bind cancer cells through RGD−integrin interactions.[31,32] In this study, RGD was used as a tumor-targeting ligand to enhance the tumor cell uptake of the nanoparticles. Moreover, to switch on the targeting property under the tumor environment, MMP substrate peptide (PLGVR) was also introduced to the nanoparticles. The component containing functional peptide sequences, N_3GPLGVRGRGDK-Ad, was assembled to MSN-SS-CD via "host−guest" interaction between Ad and β-CD (Scheme 1A). The detailed synthesis procedures of the peptide are provided in the Supporting Information. Briefly, to synthesize the peptide, Fmoc-Lys(AD)-OH was first synthesized. The structure of Fmoc-Lys(AD)-OH was confirmed by ^{1}H NMR (Figure S2). Then the peptide was prepared manually through the solid-phase peptide synthesis. The molecular weight of the component containing peptide sequences was analyzed by ESI-MS (Figure S3A). The typical absorption peak of azide moiety at 2113 cm^{-1} (Figure S1F) confirmed the successful incorporation of the peptide containing component.

After introduction of the peptide sequence to the nanoparticles, a biocompatible and degradable polyanion, PASP, was covalently coupled with azide moiety by click chemistry to form a protection layer. As shown in Scheme S2, to synthesize PASP(obzl)-alkyne, L-aspartic acid 4-benzyl ester *N*-carboxyanhydride (Asp(obzl)-NCA) was obtained by intramolecular ring closure of H-Asp(obzl)-OH. After that, propargyl amine was used as an initiator for the ring-opening polymerization of Asp(obzl)-NCA, which led to the formation of PASP(obzl)-alkyne. The molecular weight (M_w = 4211) and polydispersity index (PDI = 1.13) of PASP(obzl)-alkyne were determined by SEC-MALLS. PASP-alkyne was obtained after the deprotection of the 4-benzyl ester group under alkaline condition. The structure of PASP-alkyne was characterized by FT-IR and ^{1}H NMR (Figure S4). The absorption peak at 2120 cm^{-1} confirmed the existence of the alkyne groups. Additionally, the appearance of PASP signals (2.66 and 4.39 ppm) and the disappearance of the signals from obzl groups suggested PASP-alkyne was successfully synthesized. After introduction of PASP-alkyne to the surface of nanoparticles, MSN-SS-CD-peptide-PASP (MEMSN) was obtained. The disappearance of the typical absorption peak at 2113 cm^{-1} indicated that the azide groups on the outer surface of MSN-SS-CD-peptide were completely reacted (Figure S1). The decreased ζ potential (−25.8 mV) of DOX loaded MSN-SS-CD-peptide-PASP (Table S1) also suggested that the negatively charged PASP was successfully introduced onto the surface of nanoparticles. After being decorated with CD gatekeepers, peptides, and PASP, the obtained DOX loaded MSN-SS-CD-peptide-PASP nanoparticles did not exhibit an obvious size increase (Figure 1D). A comparison between the particle size distributions of DOX loaded MSN-SS-CD-peptide-PASP in deionized (DI) water and in PBS with 10% serum showed there was no significant difference between them (Figure S5), suggesting that no aggregation occurred in the presence of serum. From Figure 2, the weight percentages of CD, peptide, and PASP in the nanoparticles were calculated to be 5.7, 4.8, and 11.2%, respectively. The CD:peptide:PASP molar ratio was approximately 1:1:1, indicating the complete reactions between the functional groups. The surface area and pore size of different nanoparticles were determined by Brunauer−Emmett−Teller (BET) and Barrett−Joyner−Halenda (BJH) analyses. As shown in Table S2 and Figure S6, the BET pore volume and BJH pore diameter decreased during the functionalization process.

In order to evaluate the MMP-2 responsive deshielding of PASP, the *in vitro* release in the absence of MMP inhibitor and in the presence of MMP inhibitor was compared. As shown in Figure 3, MEMSN exhibited sensitive response to MMP-2 to remove PASP. Approximately 53.6% of PASP was released after incubating with MMP-2 for 4 h. In contrast, almost no PASP was released upon exposure to MMP-2 in the presence of MMP inhibitor for 120 h. These results suggested that MEMSN showed high MMP selectivity, and thus the targeting property of MEMSN could be specially switched on in tumor environments.

To investigate the tumor-triggered targeting ability of MEMSN, DOX loaded MSN-SS-CD-peptide-PASP nanoparticles were incubated with SCC-7 (squamous cell carcinoma) cells, HT-29 (human colon cancer) cells, respectively, both of which are well-known for high MMP expression.[24] As shown in Figure 4A−C, red fluorescence could be observed clearly in SCC-7 cells after 4 h incubation with MEMSN in the absence of MMP inhibitor, indicating that the particles were uptaken by the cells. This was due to the hydrolyzation of the peptide sequence PLGVR by MMP secreted by SCC-7 cells, resulting in the deshielding of PASP layer and the exposure of targeting RGD motif. In contrast, red

dx.doi.org/10.1021/ja312004m | J. Am. Chem. Soc. 2013, 135, 5068−5073

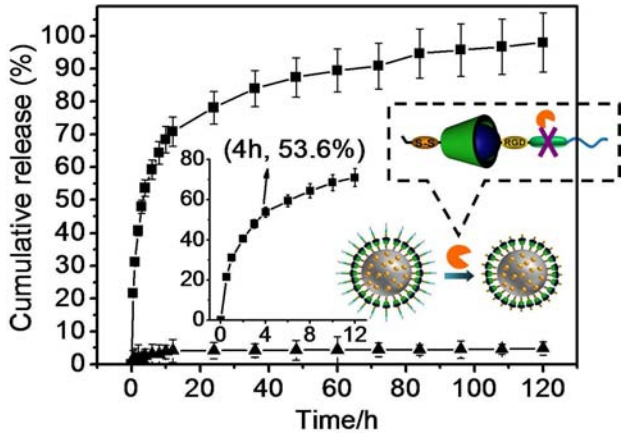

Figure 3. PASP release from unloaded MEMSN under different conditions. (■ in the presence of MMP-2 and ▲ in the presence MMP-2 and MMP inhibitor.).

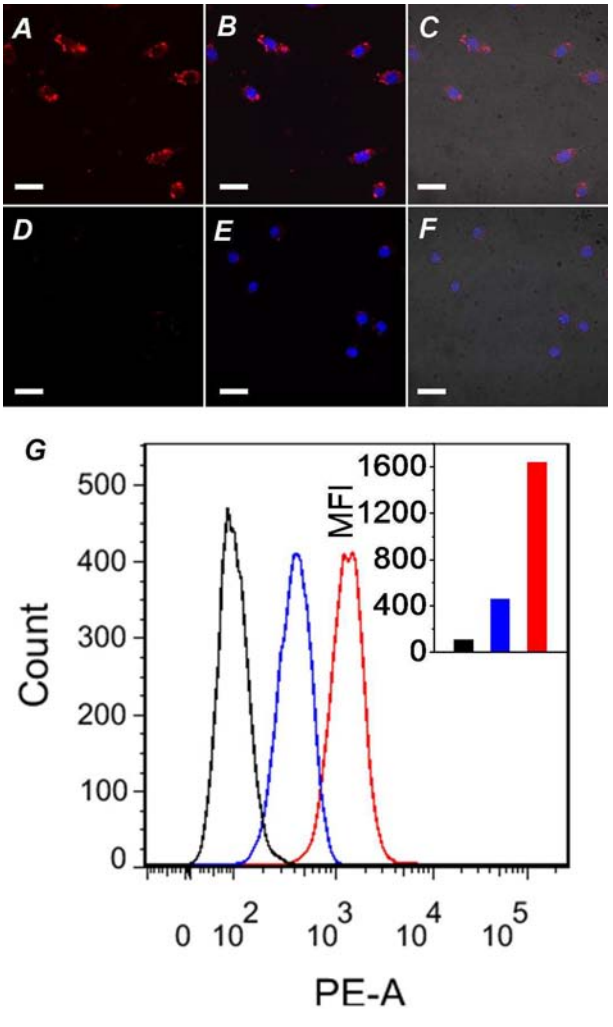

Figure 4. Confocal laser scanning microscopy (CLSM) images of SCC-7 cells treated by DOX loaded MEMSN in the (A−C) absence and (D−F) presence of MMP inhibitor. (A,D) red fluorescence images; (B,E) confocal field images; (C,F) overlap of confocal fluorescence and bright field images. (The scale bar is 50 μm). (G) Flow cytometry analysis of SCC-7 cells treated with DOX loaded MEMSN in the absence (red) and presence (blue) of MMP inhibitor and without treatment (blank).

fluorescence (due to the released DOX) can not be observed in SCC-7 cells after incubation with MEMSN in the presence of MMP inhibitor (Figure 4D,E), implying that the particles were not uptaken by the cells, which was consistent with the results shown in Figure 3, i.e., almost no PASP was removed from MEMSN in the presence of MMP inhibitor, and thus the cell uptake of the particles protected by polyanion PASP is not detectable. A similar phenomenon was observed for HT-29 cells. As shown in Figure 5, the fluorescent intensity in HT-29

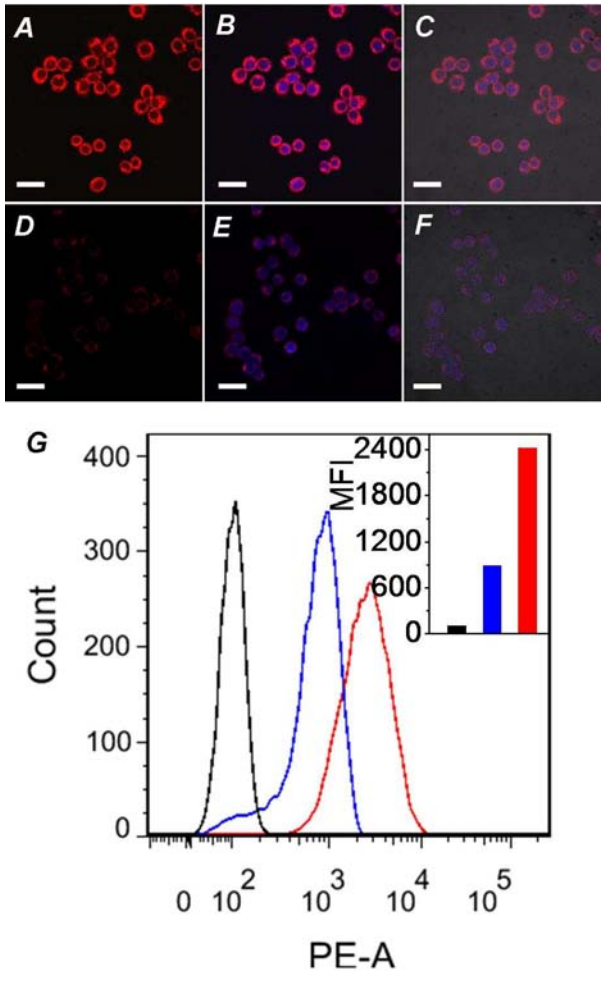

Figure 5. CLSM images of HT-29 cells treated by DOX loaded MEMSN in the (A−C) absence and (D−F) presence of MMP inhibitor. (A,D) red fluorescence images; (B,E) confocal field images; (C,F) overlap of confocal fluorescence and bright field images. (The scale bar is 30 μm). (G) Flow cytometry analysis of HT-29 cells treated with DOX loaded MEMSN in the absence (red) and in the presence (blue) of MMP inhibitor and without treatment (blank).

cells incubated with MEMSN in the absence of MMP inhibitor was dramatically enhanced, while red fluorescence was negligible in HT-29 cells in the presence of MMP inhibitor. In this study, flow cytometry analysis was used to evaluate the amount of cellular uptake of MEMSN quantitatively. As consistent with the results described above, there was 3.6- and 2.7-fold increases of mean fluorescence intensity (MFI) values in SCC-7 cells and HT-29 cells treated with MEMSN in the absence of MMP inhibitor compared with that in the presence of MMP inhibitor (Figures 4G and 5G, respectively).

dx.doi.org/10.1021/ja312004m | J. Am. Chem. Soc. 2013, 135, 5068−5073

Furthermore, to demonstrate the effect of RGD motif, a peptide sequence without RGD (N_3GPLGVRKKK-Ad, peptide*) was synthesized and anchored onto the surface of MSN-SS-CD to fabricate the particles without RGD motif (MSN-SS-CD-peptide*). The peptide molecular weight was analyzed by ESI-MS (Figure S3B). After introducing PASP-alkyne to the surface of MSN-SS-CD-peptide*, MSN-SS-CD-peptide*-PASP was obtained. The cell uptake of DOX loaded MSN-SS-CD-peptide*-PASP by SCC-7 cells and HT-29 cells was evaluated by flow cytometry analysis. As shown in Figure S7, there was a 1.7-fold increase of MFI in SCC-7 cells treated with DOX loaded MEMSN (1639 au) compared with that treated with DOX loaded MSN-SS-CD-peptide*-PASP (965 au). Similarly, there was a 1.4-fold increase of MFI in HT-29 cells treated with DOX loaded MEMSN (2413 au) compared with that treated with DOX loaded MSN-SS-CD-peptide*-PASP (1692 au). These results indicated that the existence of RGD motif improved the ability to bind with cancer cells, leading to the enhanced cell uptake.

To further confirm the cell-targeting property of MEMSN, 293T (human embryonic kidney 293 transformed) cells were also treated by DOX loaded MEMSN. As shown in Figure S8, very weak red fluorescence could be observed in 293T cells. MFI in 293T cells is much lower than that in SCC-7 cells and HT-29 cells, demonstrating that the shielding effect of the PASP layer for normal cells and the specific tumor-triggered targeting ability of MEMSN.

The *in vitro* drug release from DOX loaded MEMSN in different media is shown in Figure 6. The drug loading in

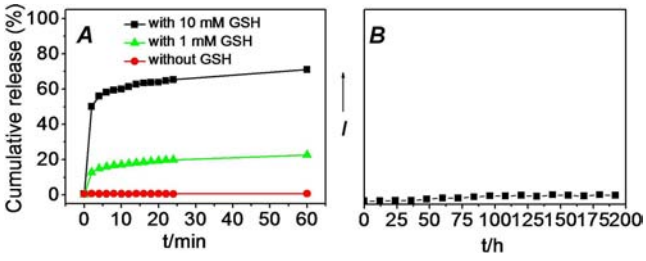

Figure 6. DOX release from DOX loaded MEMSN in PBS with (A) different GSH concentrations and (B) time-dependent fluorescence intensity during the drug release process in the absence of GSH.

MEMSN was ~4 wt % as determined by UV−vis spectroscopy. In the absence of GSH, DOX release from MEMSN was negligible for 8 days, indicating the efficient confinement of DOX in the pore reservoirs of the cores of the nanoparticles by gatekeeping of CDs. In contrast, the fast release of DOX could be detected in the presence of GSH due to the removal of CD capping via the cleavage of disulfide bonds. Moreover, the release rate increased with increasing GSH concentration. For example, about 70% of DOX was released within 1 h when the GSH concentration is 10 mM, indicating the nanoparticles could rapidly release the drug intracellularly. These results suggested that MEMSN, which allowed the glutathione-induced intracellular drug release, would not release the entrapped drugs before entering cancerous cells since the concentration of GSH in the extracellular matrix was ~10^3 times lower than that in intracellular environments.

As presented in Figure 7, the SCC-7 cell viability after treated by DOX loaded MEMSN (125 μg/mL) in the presence of MMP inhibitor was >70%. While the cell viability decreased dramatically to ~40% in the absence of MMP inhibitor. Being

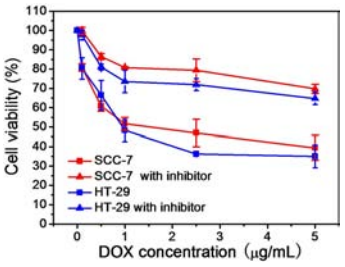

Figure 7. Viability of SCC-7 cells and HT-29 cells after being incubated with DOX loaded MEMSN in the absence or in the presence of MMP inhibitor.

consistent with the results of SCC-7 cells, the cell viability of HT-29 cells showed a similar trend. In the presence of MMP inhibitor which inhibited the effect of MMP, PLGVR sequence was stable, and the targeting motif RGD was protected by the negatively charged PASP surface layer. As a result, MEMSN was hardly uptaken by cells, and thus the corresponding cell viability was high. In contrast, in the absence of the MMP inhibitor, the cell secreted MMP could hydrolyze PLGVR to expose RGD motif, leading to the enhanced cell uptake of MEMSN followed by the accelerated drug release inside cells triggered by glutathione. To further prove the cell selectivity of MEMSN, noncancerous cells were investigated. As shown in Figure S9, the 293T cell viability after treated by DOX loaded MEMSN (125 μg/mL) was >80% due to the low uptake of MEMSN by 293T cells. These results confirmed that MEMSN was selective for cancerous cells with overexpressions of MMPs. In addition, the unloaded particles did not exhibit an obvious inhibition effect on the cell viability for all cell lines (Figure S10), confirming the decreased viability of tumor cells treated by DOX loaded MEMSN was due to the intracellular release of DOX.

■ CONCLUSIONS

In summary, we designed and fabricated a novel type of intelligent cellular-uptake-shielding MEMSN for tumor-triggered targeting drug delivery in cancerous cells. Antineoplastic drug DOX could be effectively loaded in MEMSN and released rapidly in the tumor cells due to the increased glutathione concentration. Moreover, endocytosis experiments confirmed that MEMSN acquired the ability of tumor-triggered targeting. *In vitro* results indicated that MEMSN achieved enhanced cell growth inhibition efficiency in cancerous cells. The novel multifunctional envelope-type MSN should have great potential for cancer therapy.

■ ASSOCIATED CONTENT

Supporting Information

Experimental details; synthesis and characteristic data (FT-IR and ^{1}H NMR); ζ potential of nanoparticles; size distribution of the MEMSN; BET and BJH analysis data; CLSM images and cell viability of 293T cells treated by DOX loaded MEMSN; flow cytometry analysis of SCC-7 and HT-29 cells and 293T cells treated with DOX loaded MEMSN or DOX loaded MSN-SS-CD-peptide*-PASP; and viability of SCC-7 and HT-29 cells and 293T cells after being incubated with unloaded MSN-SS-CD-peptide-PASP. This material is available free of charge via the Internet at http://pubs.acs.org.

dx.doi.org/10.1021/ja312004m | J. Am. Chem. Soc. 2013, 135, 5068−5073

AUTHOR INFORMATION

Corresponding Author

*Corresponding Author xz-zhang@whu.edu.cn

Notes

The authors declare no competing financial interest.

ACKNOWLEDGMENTS

We acknowledge the financial support from National Natural Science Foundation of China (51125014 and 51233003), Ministry of Science and Technology of China (2011CB606202), and the Fundamental Research Fund for the Central Universities (201120302020002).

REFERENCES

(1) Bakken, E. E.; Heruth, K. *Ann. N.Y. Acad. Sci.* **1991**, *618*, 422.
(2) Kogurea, K.; Moriguchib, R.; Sasakib, K.; Uenoc, M.; Futakid, S.; Harashima, H. *J. Controlled Release* **2004**, *98*, 317.
(3) Mailander, V.; Landfester, K. *Biomacromolecules* **2009**, *10*, 2379.
(4) Oupicky, D.; Ogris, M.; Howard, K. A.; Dash, P. R.; Ulbrich, K.; Seymour, L. W. *Mol. Ther.* **2002**, *5*, 463.
(5) Fischer, D.; Li, Y.; Ahlemeyer, B.; Krieglstein, J.; Kissel, T. *Biomaterials* **2003**, *24*, 1121.
(6) Ma, S. F.; Nishikawa, M.; Katsumi, H.; Yamashita, F.; Hashida, M. *J. Controlled Release* **2005**, *102*, 583.
(7) Lee, Y.; Miyata, K.; Oba, M.; Ishii, T.; Fukushima, S.; Han, M.; Koyama, H.; Nishiyama, N.; Kataoka, K. *Angew. Chem., Int. Ed.* **2008**, *47*, 5163.
(8) Gratton, S. E.; Ropp, P. A.; Pohlhaus, P. D.; Luft, J. C.; Madden, V. J.; Napier, M. E.; DeSimone, J. M. *Proc. Natl. Acad. Sci. U.S.A.* **2008**, *105*, 11613.
(9) Cho, E. C.; Xie, J.; Wurm, P. A.; Xia, Y. *Nano Lett.* **2009**, *9*, 1080.
(10) Xiao, W.; Chen, W. H.; Xu, X. D.; Li, C.; Zhang, J.; Zhuo, R. X.; Zhang, X. Z. *Adv. Mater.* **2011**, *23*, 3526.
(11) Yang, X. Z.; Du, J. Z.; Dou, S.; Mao, C. Q.; Long, H. Y.; Wang, J. *ACS Nano* **2012**, *6*, 771.
(12) Quan, C. Y.; Chen, J. X.; Wang, H. Y.; Li, C.; Chang, C.; Zhang, X. Z.; Zhuo, R. X. *ACS Nano* **2010**, *4*, 4211.
(13) Kessenbrock, K.; Plaks, V.; Werb, Z. *Cell* **2010**, *141*, 52.
(14) Vihinen, P.; Ala-aho, R.; Kahari, V. M. *Curr. Cancer Drug Targets* **2005**, *5*, 203.
(15) Aureli, L.; Gioia, M.; Cerbara, I.; Monaco, S.; Fasciglione, G. F.; Marini, S.; Ascenzi, P.; Topai, A.; Coletta, M. *Curr. Med. Chem.* **2008**, *15*, 2192.
(16) Friedl, P.; Wolf, K. *Cancer Res.* **2008**, *68*, 7247.
(17) Zhao, W.; Gu, J.; Zhang, L.; Chen, H.; Shi, J. L. *J. Am. Chem. Soc.* **2005**, *127*, 8916.
(18) Slowing, I. I.; Vivero-Escoto, J. L.; Wu, C. W.; Lin, V. S. *Adv. Drug Delivery Rev.* **2008**, *60*, 1278.
(19) Tu, H. L.; Lin, Y. S.; Lin, H. Y.; Hung, Y.; Lo, L. W.; Chen, Y. F.; Mou, C. Y. *Adv. Mater.* **2009**, *21*, 172.
(20) Barbé, C.; Bartlett, J.; Kong, L.; Finnie, K.; Lin, H. Q.; Larkin, M.; Calleja, S.; Bush, A.; Calleja, G. *Adv. Mater.* **2004**, *16*, 1959.
(21) Kim, H.; Kim, S.; Park, C. Y.; Lee, H.; Park, H. J.; Kim, C. *Adv. Mater.* **2010**, *22*, 4280.
(22) Du, L.; Liao, S. J.; Khatib, H. A.; Stoddart, J. F.; Zink, J. I. *J. Am. Chem. Soc.* **2009**, *131*, 15136.
(23) Ferris, D. P.; Zhao, Y. L.; Khashab, N. M.; Khatib, H. A.; Stoddart, J. F.; Zink, J. I. *J. Am. Chem. Soc.* **2009**, *131*, 1686.
(24) Park, C.; Kim, H.; Kim, S.; Kim, C. *J. Am. Chem. Soc.* **2009**, *131*, 16614.
(25) Lee, S.; Cha, E. J.; Park, K.; Lee, S. Y.; Hong, J. K.; Sun, I. C.; Kim, S. Y.; Choi, K.; Kwon, I. C.; Kim, K.; Ahn, C. H. *Angew. Chem., Int. Ed.* **2008**, *47*, 2804.
(26) Koo, A. N.; Lee, H. J.; Kim, S. E.; Chang, J. H.; Park, C.; Kim, C.; Park, J. H.; Lee, S. C. *Chem. Commun.* **2008**, 6570.
(27) Verma, A.; Simard, J. M.; Worrall, J. W. E.; Rotello, V. M. *J. Am. Chem. Soc.* **2004**, *126*, 13987.
(28) Oishi, J.; Ijuin, M.; Sonoda, T.; Kang, J. H.; Kawamura, K.; Mori, T.; Niidome, T.; Katayama, Y. *Bioorg. Med. Chem. Lett.* **2006**, *16*, 5749.
(29) Hood, J. D.; Cheresh, D. A. *Nat. Rev. Cancer* **2002**, *2*, 91.
(30) Hart, S. L.; Harbottle, R. P.; Cooper, R.; Miller, A.; Williamson, R.; Coutelle, C. *Gene Ther.* **1995**, *2*, 552.
(31) Pasqualini, R.; Koivenen, E.; Ruoslahti, E. *Braz. J. Med. Biol. Res.* **1996**, *29*, 1151.
(32) Ruoslahti, E. *Annu. Rev. Cell Dev. Biol.* **1996**, *12*, 697.